Peptide-Derivatized Shell-Cross-Linked Nanoparticles. 2. Biocompatibility Evaluation

Matthew L. Becker,*[,†,‡] LeeAnn O. Bailey,[‡] and Karen L. Wooley*[,†]

Center for Materials Innovation and Department of Chemistry, Washington University, One Brookings Drive, St. Louis, Missouri 63130, and National Institute of Standards and Technology, Polymers Division, Biomaterials Group, Gaithersburg, Maryland 20899-8543. Received March 4, 2004; Revised Manuscript Received April 26, 2004

The conjugation of the protein transduction domain (PTD) from the HIV-1 Tat protein to shell cross-linked (SCK) nanoparticles is a method to facilitate cell surface binding and transduction. In the previous report, the preparation, derivatization, and characterization of peptide-functionalized SCK nanoparticles were reported in detail. Following assembly, the constructs were evaluated in vitro and in vivo to obtain a preliminary biocompatibility assessment. The effects of SCK exposure on cell viability were evaluated using a metabolic 3-(4,5-dimethylthiazol-2-yl)-2,5-diphenyl-2*H*-tetrazolium bromide (MTT) and a fluorescent apoptosis assay. Furthermore, stages of apoptosis were quantified by flow cytometry. Although higher levels of peptide functionalization resulted in decreased metabolic function as measured by MTT assay, significant apoptosis was not observed below 500 mg/L for all the samples. To evaluate the potential immunogenic response of the peptide-derivatized constructs, a real-time polymerase chain reaction (RT-PCR) system that allows for the in vitro analysis and quantification of the cellular inflammatory responses tumor necrosis factor alpha (TNF-α) and interleukin-1 beta (IL1-*β*) was utilized. The inflammatory response to the peptide-functionalized SCK nanoparticles as measured by RT-PCR show statistically significant increases in the levels of both TNF-α and IL1-*β* relative to tissue culture polystyrene (TCPS). However, the measured cytokine levels did not preclude the further testing of SCKs in an in vivo mouse immunization protocol. In this limited assay, measured increases in immunoglobulin G (IgG) concentration in the sera were minimal with no specific interactions being isolated, and more importantly, none of the mice (>50) subjected to the three 100 *μ*g immunization protocol have died. Additionally, no gross morphological changes were observed in postmortem organ histology examinations.

INTRODUCTION

New synthetic methodologies (*1*−*3*) are enabling remarkable advances in the rational design of polymeric materials that actively control cellular and physiologic responses. These methods produce well-defined materials that are incorporated into scaffolds capable of performing specific functions while being minimally detrimental to normal cellular processes and surrounding tissues for use in therapeutic (*4*−*6*), drug delivery (*7*−*10*), and tissue engineering applications (*11, 12*). One of the critical challenges in clinical medicine currently under intense investigation is the efficient delivery of macromolecules into cells for the purposes of drug, gene, and cancer therapies (*13, 14*). In the previous article of this issue, the preparation, characterization, and biological evaluation of peptide-functionalized shell-cross-linked (SCK) nanoparticles are reported. SCK nanoparticles (*15, 16*) are micellar assemblies of amphiphilic copolymers that have been stabilized through the incorporation of covalent cross-links in the shell layer (*17*). Syntheses of complex block copolymer precursors have afforded control over the physicochemical properties of the respective nanoparticle domains (*6*, *18*, *19*). Surface charge (*20*) and functionality are controlled easily and can be tailored for specific applications (*21*). The protein transduction domain (PTD) of HIV-1 Tat (*22, 23*) has been shown to shuttle much larger molecules into cells independent of classical endocytosis (*24*) which affords intracellular access to living cells for nuclear targeting strategies (*25*), gene (*14, 26*), radiotherapies (*27*−*29*) and other purposes. The attachment of increasing numbers of protein transduction domain (PTD) motifs to SCK nanoparticles is being investigated as a method to increase the efficiency of cell-penetrating transduction. Further extension of the peptide-derivatized conjugates into biological applications requires the elucidation of how increasing peptide functionality affects the biocompatibility of the derivatized nanostructures, including the cellular apoptosis and inflammatory responses. The effects on cell viability are evaluated by metabolic and flow cytometry assays. Measuring the effects of foreign substances on in vitro cell viabilities is typically accomplished by the exposure of a cell population to the conjugate and then monitoring the enzymatic reduction of MTT to formazan in the mitochondria of living cells (*30*). The viability is then expressed as a percentage of

* To whom correspondence should be addressed. K.L.W.: Tel. (314) 935-7136, fax (314) 935-9844, e-mail: klwooley@artsci.wustl.edu. M.L.B.: Tel. (301) 975-6842, e-mail: mlbecker@nist.gov.

† Washington University.

‡ National Institute of Standards and Technology.

[1] Abbreviations: ATCC, American Type Culture Collection; CHO, chinese hamster ovary; ELISA, enzyme-linked immunosorbent assay; FMOC, 9-fluorenylmethyloxycarbonyl; HBSS, Hanks buffered salt solution; IgG, immunoglobulin G; IL, interleukin; MTT, 3-(4,5-dimethylthiazol-2-yl)-2,5-diphenyl-2*H*-tetrazolium bromide; PBS, phosphate-buffered saline; PS, phospholipid phosphatidylserine; PTD, protein transduction domain; RPMI, Roswell Park Memorial Institute; RT-PCR, real-time polymerase chain reaction; SCK, shell-cross-linked nanoparticle; SDS, sodium dodecyl sulfate; TNF, tumor necrosis factor.

10.1021/bc049945m CCC: $27.50
Published on Web 06/16/2004

cells that are dead as a function of the nanoparticle concentration. Another method to measure cell viability is an apoptosis assay, which is a technique that monitors cell membrane translocation events and the accessibility of nuclear material in response to extracellular perturbations, and the various stages of apoptosis are then quantified by flow cytometry. The ability to monitor the emission wavelengths of the respective fluorophores affords flow cytometry the ability to discriminate and quantify distinct populations of cells (*31*). It is anticipated that the two techniques will provide a complementary and accurate assessment of the effects of SCK exposure on cell viability.

Measurement of the acute inflammatory reaction in response to peptide-derivatized SCK nanoparticle exposure is another critical component in the assessment of the biocompatibility. Inflammation is characterized by the regulation of cytokines, which are responsible for the initiation, mediation, and propagation of the inflammatory response including lymphocyte activation, proliferation, differentiation, angiogenesis, and apoptosis (*32*). Quantifying the regulatory profile of cytokines at the protein level is difficult due to small sample sizes, which has created a need for alternative measurement methods. The measurement of mRNA levels is used widely to investigate the cytokine profiles at sites of inflammation (*32*). There are several techniques, aside from PCR-based methodologies, used commonly to quantify mRNA expression including Northern blotting, in situ hybridization, RNase protection assays, and cDNA arrays, each of which is limited by low measures of sensitivity (*33, 34*). Real-time polymerase chain reaction (RT-PCR) is a method for enzymatically amplifying defined sequences of mRNA, and it is the most sensitive, accurate, and adaptable of the mRNA quantitative techniques (*33, 35*). Quantitative RT-PCR has the advantage of being extremely sensitive over a large range of quantification, requires no post-PCR sample handling (*36, 37*), and has previously afforded measurement of the genetic regulatory profiles for inflammatory cytokines in response to synthetic materials (*38, 39*). Herein, a preliminary biocompatibility assessment of peptide-derivatized SCK nanoparticles is described in detail including enzymatic and apoptosis assays, which measure the effects of SCK exposure on cellular viability. In addition, RT-PCR measurements were used to quantitatively assess the inflammatory response caused by the peptide-functionalized nanoparticles. Following in vitro testing methodologies, a three-month mouse immunization protocol involving multiple booster immunizations found minimal increases in IgG levels in the serum and furthermore elucidated no specific immunogenic response. The initial biocompatibility evaluation of peptide-functionalized SCK nanoparticles described in this article, while limited in scope, is a critical first step toward the identification of potentially detrimental interactions between biological species and SCK nanoparticles. Furthermore, these in vitro assays and limited in vivo studies provide justification for additional animal studies, including biodistribution and liver function assays, which are crucial to efforts to develop in vivo therapeutic applications.

EXPERIMENTAL PROCEDURES

Materials. FMOC-protected amino acids and preloaded solid-phase Wang resins were purchased from NovaBiochem-CalBiochem Corp (San Diego, CA). Sodium dodecyl sulfate (SDS), 3-(4,5-dimethylthiazol-2-yl)-2,5-diphenyl-2*H*-tetrazolium bromide (98%) (MTT), Tween20, mouse IgG (Fc, Sigma I-8765), and goat anti-mouse IgG alkaline phosphatase conjugate (Fc specific, Sigma A-1418) were purchased from Sigma (St. Louis, MO). Alkaline phosphate substrate solution was purchased from BioRad (Hercules, CA). Spectra/Por dialysis membranes (Spectrum Laboratories, Inc., Rancho Dominguez, CA), 96-well polystyrene plates (Falcon), and ELISA plates (Nunc-Immuno, Maxisorp) were purchased from Fisher Scientific Company (Pittsburgh, PA). QuantiTect SYBR Green RT-PCR Kit and Rneasy Kit were obtained from Qiagen (Valencia, CA). Primer identification, isolation, and probe development were nearly identical to methods described previously (*38, 39*).

Certain commercial materials and equipment are identified in this paper in order to specify adequately the experimental procedure. In no case does such identification imply recommendation by the National Institute of Standards and Technology nor does it imply that the material or equipment identified is necessarily the best available for this purpose.

The Animal Facility at the Washington University Department of Biology handled immunizations, sera collections, and organ histology. Animal studies were conducted under Protocol 20010343 approved by the Animal Studies Committee of Washington University.

Cell Lines. Mouse myeloma B cells (ATCC, Manassas, VA) CRL-1581.1 and CHO cells (ATCC) were obtained as gifts from Professor Jacob Schaefer (Washington University, St. Louis, MO). Mouse myeloma B cells were cultured in RPMI (Life Technologies, Rockville, MD) 1640 media using TCM serum replacement (10%, volume fraction) obtained from Celox Laboratories (St. Paul, MN). RAW 264.7 cells were purchased from ATCC. RAW 264.7 and CHO cells were maintained in RPMI supplemented with 10% (volume fraction) heat-inactivated fetal bovine serum (FBS, Life Technologies, Rockville, MD), in 5% CO_2:95% air (volume fractions) at 37 °C. To harvest, RAW 264.7 cells were washed with calcium- and magnesium-free phosphate-buffered saline and subsequently incubated with HBSS to promote release from the flask.

Determining Cell Viability via MTT Assay. Mouse myeloma B cells were counted and diluted into fresh media at concentrations of 50 000 cells/mL and an aliquot (100 μL) was seeded to each well in a 96-well plate. After deposition of the cell suspension, the plates were placed in an incubator (37 °C, 5% CO_2, volume fraction) and allowed to grow for 24 h. Fresh 96-well plates were loaded with sterile buffer (40 μL), and the first column of each row was loaded with polymer or SCK stock solutions of known concentration. The first columns in each plate were then diluted serially from columns 2 to 11. The last columns were held as controls with no polymer or SCK added. Fresh media (50 μL) was then added to every well in the plates. The original plates were removed from the incubator, and the premixed sample solutions were added to the corresponding wells in each plate. After 24 h incubation, the inoculated plates were removed from the incubator, and an aliquot of MTT (Sigma) (20 μL, 5.00 mg/mL) in PBS (0.05 mol/L phosphate, 0.05 mol/L sodium chloride, pH 7.4) was added to each well. The plates were returned to the incubator and allowed to equilibrate for 2 h. After 2 h, extraction buffer (80 μL, 20% (mass fraction) SDS (Sigma) in 50:50 DMF:H_2O, volume fraction, pH 4.7) was added to each well to extract the aqueous insoluble formazan product. The plates were then returned to the incubator for 18 h to allow for the extraction after which the absorbance of each solution was measured at 560 nm. Concentrations were determined by the weight of lyophilized polymer sample dissolved in PBS and then adjusted for the dilution of

the media. Results are an average of four values, and the standard deviation is reported for each concentration.

Apoptosis Assay. Apoptotic analysis of RAW 264.7 cells was assessed using the Guava Nexin Kit (Guava Technologies, Hayward, CA). RAW 264.7 cells were plated in 12-well plates at 50 000 to 100 000 cells per well and allowed to adhere for 24 h, after which the cells were inoculated with 100 μL aliquots of the respective samples. The initial quantity of SCK was suspended in 0.500 of PBS. The respective samples were subsequently added to RAW 264.7 cultures (100 μL). After 24 h, the media was removed from the cells, and the cultures were washed with PBS. To promote release from the plate, the cells were incubated with 1 mL of HBSS for 30 min. The cells were then gently removed from the plate, and the volume was adjusted to 300 μL. The cell suspension was incubated with 5 μL of Nexin 7-AAD and 5 μL of Annexin V−PE for 5 min in a light-protected environment and subsequently analyzed.

Flow Cytometry. Apoptotic analysis of RAW 264.7 cells incubated on the thin films or in the presence of the nanoparticles was assessed using the Guava Nexin Kit (Guava Technologies, Hayward, CA). RAW 264.7 cells were plated in 24-well plates (50 000 to 100 000) cells per well and allowed to adhere on tyrosine-derived polycarbonate thin films or tissue culture polystyrene for 24 h prior to analysis by flow cytommetry. Full experimental details were described previously (*38, 39*).

mRNA Extraction. Cells were plated in sterile 150 mm × 25 mm nonpyrogenic polystyrene dishes (Daigger, Vernon Hills, IL). SCK nanoparticles were added to plated cells 24 h following seeding. The mRNA extraction was carried out using the materials and protocol provided in the Rneasy Kit from Qiagen (Valencia, CA). The mRNA extraction protocol was followed according to the manufacturer's specification, except a 21-gauge needle was used to homogenize the sample. The RNA was treated with RNA Secure immediately following elution and stored at −20 °C. Standard spectrophotometric measurements were taken, and a 2% (mass fraction) agarose gel stained with 10 μg/mL ethidium bromide (Sigma, St. Louis, MO) was used to image the RNA. Densitometry was performed using the Versa Doc imaging system (Bio-Rad, Hercules, CA).

Standards. The plasmids containing the cDNA inserts for TNF-α, IL-1β, and the18 S ribosomal subunit were purchased from ATCC. The plasmids were grown in *luria-bertani* (LB) medium (ATCC, medium 1065) with 100 μg/mL of ampicillin for selection purposes. Plasmid DNA was isolated using the Plasmid Giga Kit (Qiagen, Valencia, CA) following the manufacturer's protocol. Spectrophotometric measurements were made at 260 nm, and a 1% (mass fraction) agarose gel stained with 10 μg/mL ethidium bromide (Sigma, St. Louis, MO) was used to image the DNA. Densitometry was performed using the Versa Doc imaging system (Bio-Rad, Hercules, CA).

Primer Design. Primers were designed using Primerfinder (Whitehead Institute for Biomedical Research) for the RT-PCR experiments. The primers generated were used in both PCR and RT-PCR experiments. They are as follows:

18S: 5′ agcgaccaaaggaaccataa 3′ and 3′ ctcctcctcctcctctctcg 5′

TNF-α: 5′ tttcctcccaataccccttc 3′ and 3′ agtgcaaaggctccaaagaa 5′

IL-1β: 5' tgtgaaatgccacctttga 3' and 3' gtagctgccacagcttctcc 5'

The amplicons generated from these primers are 204 base pairs, 202 base pairs, and 205 base pairs, respectively. DNA sequencing was performed using the Big Dye Terminator Kit (ABI, Foster City, CA) on a 310 DNA Genetic Analyzer (ABI, Foster City, CA).

RT-PCR. RT-PCR was carried out using the Quanti-Tect SYBR Green RT-PCR Kit and protocol (Qiagen, Valencia, CA). All RT-PCR experiments were performed using the iCycler (Bio-Rad, Hercules, CA). The protocol utilizes the following thermal parameters: Reverse Transcription: 30 min at 50 °C. Activation step: 15 min at 95 °C. Three-step cycling: denaturation for 30 s at 95 °C, annealing for 2 min at 57 °C, extension for 2 min at 72 °C for 45 cycles. A melt curve was subsequently performed to analyze the products generated, which began at 50 °C and increased to 95 °C in 1 °C increments.

Immunization of Mice. For each sample, five mice (female, balb c, 7 weeks old) were inoculated with 100 μL of polymer or SCK solution (1 mg/mL in PBS) at (0, 4, and 8) weeks. The mice were bled for preimmunoserum screening prior to the primary injection. Blood samples were then collected 14 d after (4 and 8)-week booster immunizations, respectively. Serum was obtained after clotting at 4 °C, for 24 h, and centrifugation. Serum samples were stored at −20 °C in small aliquots for later use.

Determining Antibody Titer by ELISA Assay. Samples for ELISA for the five mice were first prepared by dilution in five 96-well plates. PBS buffer (100 μL) was added to each well in the plates. The serum vials were thawed, and each serum sample (5 μL) was diluted 1:100 in PBS and was transferred, in quadruplicate, in aliquots (100 μL) to the first four wells in the top row of each corresponding plate. The serum obtained following the first booster immunization was added to the next four wells, and the serum obtained following the second booster immunization was added to the final four wells, columns 9 to 12. The serum was then serially diluted 2-fold in rows 2−7 in each plate. Following dilution, 100 μL from each well was transferred to a corresponding ELISA (Nunc-Immuno, Maxisorp) plate and incubated overnight at 4 °C. The wells were washed three times with PBS buffer (300 μL) containing 0.05% (mass fraction) Tween 20 (Sigma), and the remaining binding sites on the plates were blocked with sodium caseinate (100 μL, 2.5%, mass fraction, in PBS) followed by overnight incubation at 4 °C. The wells were again washed three times, and a 1:40 000 dilution of goat anti-mouse IgG alkaline phosphatase conjugate (100 μL, Sigma) was added to each well and allowed to incubate for 1 h at room temperature before being washed five times. Alkaline phosphatase substrate solution (100 μL, BioRad) was added to each well. Color development was allowed to take place for 30 min and then was quenched with 4 mol/L H_2SO_4 (50 μL per well). Absorption measurements were made at 405 nm. To determine the absolute antibody concentrations, mouse IgG standards were run in parallel with each ELISA plate. Serial dilutions of mouse IgG (from 5.00 to 0.08 μg/mL) were used to generate the linear calibration plot of absorbance vs concentration. The value corresponding to 0 μg/mL was the background reading and was subtracted from all samples.

RESULTS AND DISCUSSION

The assessment of material biocompatibility is a complicated process, which includes both in vitro and in vivo measurement methods, each of which depend on the physical and chemical nature of the material and the nature of the biological interaction. Surface characteristics such as hydrophobicity, morphology, surface charge, and chemical functionality are all known to play key roles

Table 1. PTD-Derivatized SCK Characterization Data

no.	sample composition	no. of peptides nominal	no. of peptides UV−vis	no. of peptides phenylglyoxal	zeta (mV)	DLS D_n (nm)
5	micelle	0	0	0	−27 ± 0.7	38 ± 3
6	SCK	0	0	0	−20 ± 0.5	37 ± 2
7	0.5% PTD SCK	52 ± 2	38	41	−28 ± 0.9	35 ± 3
8	1.0% PTD SCK	104 ± 4	87	83	−23 ± 0.7	36 ± 3
9	2.0% PTD SCK	210 ± 10	~500	202	−22 ± 0.5	32 ± 4

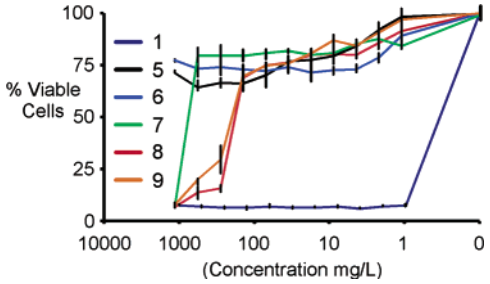

Figure 1. The conjugation of the PTD sequence to the SCKs has dramatic effects on the resulting cell viability. The 2.0% PTD-functionalized SCK **9** is toxic to the cells between 7 mol/L to 13 mol/L in PTD. The 0.5% and 1.0% PTD-functionalized SCKs (**7** and **8**) are toxic between 14 mol/L to 28 and 7 mol/L to 15 mol/L in PTD, respectively. The parent micelles and SCKs (**5** and **6**) did not affect the viability of the cells at any measured concentration. Error bars are representative of one standard deviation from the mean of quadruplicate samples harvested from four separate wells of mouse myeloma B cells and are the estimates of the standard uncertainties.

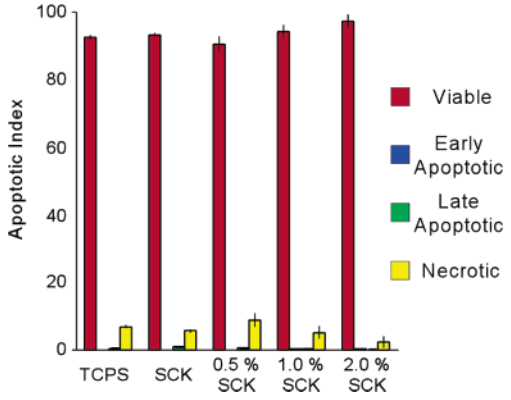

Figure 2. Four distinct populations of cells can be identified with flow cytometry. Viable cells: Annexin V (−) and 7-AAD (−); early apoptotic cells: Annexin V (+) and 7-AAD (−); late stage apoptotic: Annexin V (+) and 7-AAD (+); necrotic: Annexin V (−) and 7-AAD (+). Error bars are representative of one standard deviation from the mean of triplicate samples, each harvested from three separate populations of RAW 264.7 cells, and are the estimates of the standard uncertainties.

in governing cell adhesion and proliferation (*40*). Several physicochemical parameters for the PTD-derivatized SCK nanoparticles whose syntheses and characterization are described in the previous article of this issue are outlined in Table 1. However, a clear framework outlining the critical physiochemical and surface-mediated interactions within which to facilitate the development of materials minimally detrimental to cells does not exist. For applications concerning the delivery of macromolecules into cells, the enhanced efficiency of conjugate transduction must be weighed against any detrimental biological interactions including effects on both cell viability and immune response. The cell viabilities in the presence of the peptide-derivatized polymeric constructs were evaluated by MTT assay (*30*), which monitors enzymatic activity of a cell organelle (in this case mitochondria), and flow cytometry. Previously, the protein transduction sequence has been used at concentrations of up to 100 μmol/L without affecting the viability of certain cell lines (*41*).

As illustrated by the data of Figure 1, the PTD sequence, with four additional glycine residues, was found to decrease the enzymatic reduction of MTT in the mitochondria of mouse myeloma B cells at approximately 110 μmol/L concentrations. In contrast, the viabilities of the cells upon exposure to buffered solutions of micelles or SCKs remain (70 to 90) % at concentrations above 100 mg/L. The small drop in viability is due primarily to the dilution of the media as shown by control experiments in which buffer and no buffer were added to different cell populations. Exposure of the cells to the parent PAA_{56}-*b*-PMA_{185} micelles, **5**, and the corresponding unfunctionalized SCK, **6**, did not affect cell viability up to 1125 mg/L concentrations. However, the derivatization of the nanoparticle with increasing numbers of the PTD sequence has a significant effect on the viability of the cell populations as measured by the enzymatic function. The 2.0% PTD-functionalized SCK **9** is toxic to the cells between (140 and 280) mg/L (7 μmol/L to 13 μmol/L in PTD). The 0.5% and 1.0% PTD-functionalized SCKs (**7** and **8**) are toxic between (560 and 1125) mg/L (14 μmol/L to 28 μmol/L and 7 μmol/L to 15 μmol/L in PTD, respectively). The mechanism of toxicity has not been determined.

In addition to the MTT enzymatic assay, the peptide-derivatized nanoparticles have been evaluated by a fluorescent flow cytometry experiment to determine the effects of incubation with SCKs upon the induction of apoptosis. Apoptosis is characterized by numerous morphological changes, the first of which involves the translocation of phosphatidylserine (PS) from the inner to the outer surface of the cellular plasma membrane. Once exposed to the extracellular environment, PS sites are accessible to Annexin V, a phospholipid binding protein with a high affinity for PS. For measurement purposes, Annexin V is conjugated to FITC and used for the identification of cells in the early stages of apoptosis via flow cytometry. Because PS binding sites are also accessible when the cells are in a necrotic state, Annexin V is not an absolute marker of apoptosis. Therefore, it is often used in conjunction with 7-aminoactinomysin, (7-AAD) which binds to exposed nucleic acids, when the cell membrane integrity is compromised. Cells that are negative (unstained) for both Annexin V and 7-AAD have no indications of apoptosis: PS translocation has not occurred, and the plasma membrane remains intact. Cells that are Annexin V (+) and 7-AAD (−), however, are in early apoptosis, as PS binding sites are exposed, but the plasma membrane is still intact. Cells that are (+) for both Annexin V and 7-AAD are either in the late apoptosis (irreversible) stage or are not viable. The flow cytometry data shown in Figure 2 indicate that the SCKs do not induce apoptosis at the concentrations tested. The total inoculated concentration was 0.5 mg/mL (500 mg/L) for each SCK sample. In addition, a visual assessment of the effects of exposure to PTD-derivatized SCKs at the 5 day time point indicated that the nanoparticles did not affect the continued growth of the cells nor did they

induce significant morphological changes (data not shown). These results are comparable to the MTT assay results. Although the MTT assay depicts a shutdown in mitochondrial function at certain concentrations, exposure of each of the samples to the cells at concentrations of 500 mg/L did not lead to cellular apoptosis.

Immunogenicity Results. The extent of PTD functionality is of significant importance as it may affect the immune response. The nature of the response has significant clinical implications, as severe inflammatory responses may prevent in vivo applications. Recent literature has reported that the addition of HIV Tat PTD enhances minigene epitope presentation in tissue culture, but the attachment of PTD to full-length proteins does not enhance the immune response of the construct (*42*). The reported data were for a 1:1 stoichiometry of PTD: protein, and it is unclear whether the presentation of multiple copies of the sequence on the surface of an SCK would have a synergistic or negligible effect on the cellular immune response. The initiation and propagation of an immune response is ultimately regulated by cytokines. Cytokines are the primary mediators of a host immune response and are able to both induce apoptosis and modulate survival through the activation of genes in response to bacterial toxins, inflammatory products, and other invasive stimuli (*43*). Two of the most important cytokines in the acute inflammatory response are tumor necrosis factor alpha (TNF-α) and interleukin-1 beta (IL1-*β*) (*44*). TNF-α is synthesized and secreted by macrophages. TNF-α is part of a complex network of cytokines and is capable of initiating cascades, which control the synthesis and expression of signaling molecules, hormones, and their receptors (*45*−*47*). Knowledge of the cellular cytokine profile is key to identifying the processes involved in the immune response (*48*) and crucial to the further elucidation on the physicochemical properties of the bioconjugate that are inducing the response. Another prominent cytokine involved in the inflammatory responses is interleukin-1 (IL-1). Although IL-1 protects the organism by enhancing the response to pathogens and initiating healing process, its overproduction can induce numerous pathological consequences including septic shock and leukemia (*21*). The measurement of mRNA levels has been used widely to measure cytokine proliferation, which is responsible for the initiation, mediation, and propagation of cellular inflammatory responses (*32*). The genetic expression profiles of IL-1*β* and TNF-α have been measured by real-time polymerase chain reaction (RT-PCR) (*49*). In this study, the mRNA profiles of TNF-α and IL-1*β* in response to PTD, SCKs, and SCKs derivatized with increasing amounts of PTD sequences were investigated using RT-PCR. In the previous manuscript of this issue, PTD was conjugated in (0.005, 0.01, and 0.02) molar ratios, relative to the acrylic acid residues in the shell, to the SCK nanoparticles resulting in SCK populations nominally possessing 52, 104, and 210 (41, 83, and 202 as measured by phenylglyoxal) PTD peptides per particle, respectively. RAW 264.7 cells were used because they retain the characteristics of primary cultured macrophages in vitro, including the ability to release cytokines (*50*−*53*). Cells were exposed to the respective SCK nanoparticle samples by adding the conjugates to the murine macrophages 24 h following seeding. After a 24 h incubation period, the mRNA was extracted from the cell populations. Using a reverse transcriptase enzyme, mRNA is converted to the cDNA template necessary for amplification. Once cDNA is generated, gene specific primers, a DNA polymerase, and a fluorescent moiety are utilized to amplify and label

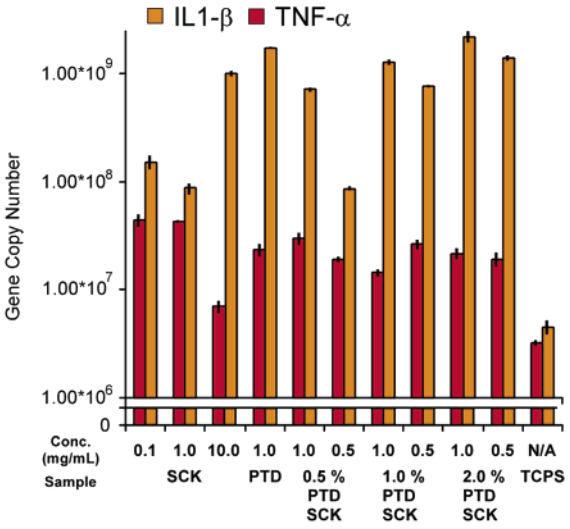

Figure 3. Genetic cellular inflammatory responses exhibited 24 h after incubation with different concentrations of peptide-functionalized SCK nanoparticles were quantified by RT-PCR. The data depict minimal increases in the production of TNF− and an elevation in the levels of IL-1 relative to tissue culture polystyrene. Error bars are representative of one standard deviation from the mean of triplicate samples, each harvested from three separate populations of RAW 264.7 cells, and are the estimates of the standard uncertainties.

the amplicon generated. The gene product accumulation was then measured during the exponential phase of the amplification reaction (*36*). The copy number from each of the samples was obtained by extrapolating to a standard gene curve of known concentration and copy number to yield quantitative data. The assay also includes the analysis of mRNA that does not change in relative abundance (18S) during the course of treatment to serve as an internal control (*54*). The genetic profiles of the inflammatory response to SCKs (**1**−**3**), PTD (**4**), PTD-functionalized SCK nanoparticles (**5**−**10**), and tissue culture polystyrene (TCPS, **11**) are shown in Figure 3.

TNF-α mRNA synthesis was up-regulated 2-fold to 14-fold (depending on concentration) in response to exposure of the parent SCK nanoparticle, **6**, over TCPS. It is interesting to note that the highest concentration, 10.0 mg/L, of the parent SCK **6** actually caused less of an increase, 2.2-fold, than lower concentrations, 0.1 and 1.0 mg/L, of SCK **6**, 13.5-fold and 13.2-fold, respectively. When looking at the effects of parent SCK concentration on TNF-α production, the difference between (0.1 and 1.0) mg/mL are statistically insignificant, while the 10.0 mg/mL sample measures 6.1-fold less than at the 1.0 mg/mL level. Interestingly, the down-regulation of TNF-α has been demonstrated previously in liposome vectors formulated with cationic lipids (*55*). The measured TNF-α levels for the PTD-functionalized SCKs are less than the levels of the parent SCK in all cases (1.5-fold to 3.0-fold) and show no concentration or functionality dependence. The levels of TNF-α measured in response to the peptide-functionalized nanoparticles, regardless of the extent of derivatization and concentration tested, are statistically insignificant when compared to the levels induced by the PTD domain itself. The copy numbers, fold increases, and the p values ($p < 0.05$ significant at 95% confidence, derived from the students t-test) indicating statistical significance are listed in Table 2.

The measured increases of IL1-*β* production in response to PTD-, SCK-, and PTD-functionalized SCKs are much more pronounced than the copy number levels of TNF-α as compared to TCPS. The measured levels range

Table 2. Nanoparticle Concentration, Copy Number Identification, and Evaluation of Statistical Significance[a]

			gene copy number		increase over TCPS		increase over PTD		increase over SCK (**2**)	
no.	sample composition	concentration mg/mL	TNF-α	IL1-β	TNF-α p(95%)	IL1-β p(95%)	TNF-α p(95%)	IL1-β p(95%)	TNF-α p(95%)	IL1-β p(95%)
1	SCK	0.1	4.33×10^7	1.52×10^8	13.5	33.4	1.9	(11.2)	1	1.8
					0.0067	0.0076	0.0136	0.0003	*0.8499*	0.0177
2	SCK	1.0	4.25×10^7	8.65×10^7	13.2	18.8	1.8	(19.8)	1	1
					0.0007	0.0054	0.0027	0.0001		
3	SCK	10.0	7.01×10^6	1.01×10^9	2.2	221.9	(3.3)	(1.7)	(6.1)	11.7
					0.0241	0.0011	0.0170	0.0003	0.0001	0.0014
4	PTD	0.1	2.30×10^7	1.71×10^9	8.6	375.8	1	1	(1.8)	19.8
					0.0089	0.0001			0.0027	0.0001
5	0.5% PTD SCK	1.0	2.93×10^7	7.06×10^8	9.1	155.2	1.3	(2.4)	(1.5)	8.2
					0.0067	0.0005	*0.25*	0.0011	0.0103	0.0010
6	0.5% PTD SCK	0.5	1.88×10^7	8.59×10^7	5.8	18.9	(1.2)	(19.9)	(2.3)	1
					0.0018	0.0008	*0.19*	0.001	0.0041	*0.9404*
7	1.0% PTD SCK	1.0	1.42×10^7	1.27×10^9	4.4	279.1	(1.6)	(1.3)	(3.0)	14.7
					0.0045	0.0015	*0.0598*	0.0164	0.0033	0.0018
8	1.0% PTD SCK	0.5	2.60×10^7	7.57×10^8	8.0	166.4	1.1	(2.3)	(1.6)	8.8
					0.0053	0.0002	*0.4806*	0.0007	0.0214	0.0005
9	2.0% PTD SCK	1.0	2.15×10^7	2.20×10^9	6.7	483.5	(0.9)	1.3	(2.0)	25.4
					0.0067	0.0049	*0.6930*	0.0890	0.0123	0.0053
10	2.0% PTD SCK	0.5	1.91×10^7	1.38×10^9	5.9	303.3	(0.8)	(1.2)	(2.2)	16.0
					0.0090	0.0007	*0.3600*	0.0206	0.0100	0.0009
11	TCPS	N/A	3.22×10^6	4.55×10^6	1	1	-	-	-	-

[a] Parentheses indicate decreases in copy number, and italic numbers denote comparisons that are statistically insignificant.

from 18.8-fold to 483.5-fold increases over TCPS and 1-fold to 25.4-fold increase over SCKs of similar concentration and show statistical dependence with regard to both concentration and PTD functionalization. The differences in TNF-α and IL1-β expression measured in this series reflect different pathways of signal transduction (*56*) with regard to both the time frame and the severity of the response (*31, 38, 57, 58*) to the respective inflammatory stimuli.

Following the in vitro measurements on cell viability and inflammatory response, the SCKs and PTD-derivatized SCKs were then tested in vivo to gauge their immunogenic response in balb c mice. Enzyme-linked immunosorbent assays (ELISA) were used to quantify the increases in IgG production in response to immunization with the test compounds. Efforts to isolate specific responses by plating the SCKs on the ELISA plate prior to serum incubation were not successful due to an insignificant specific antibody response. This result can be attributed to two possible factors: (1) the nanoparticles could induce a nonspecific immune response, and (2) the sera used for the ELISA measurements were collected 14 d following the respective immunization, a sufficiently long time that any acute inflammatory response may have passed. We therefore decided to look at the increases in IgG concentration on an individual mouse basis to look for relatively large increases. Figure 4 shows the three antibody titers determined for each mouse in the study. The PTD peptide by itself is not immunogenic after two booster immunizations, and the parent SCKs possessing poly(acrylic acid-*co*-acrylamide) shells display negligible values of titer increases over the control PBS injections. Those SCKs possessing various amounts of PTD functionality, 0.5%, 1.0%, and 2.0% (**7**, **8**, and **9**), qualitatively showed a general trend of increasing antibody titer in the serum with increasing degrees of nanoparticle functionalization. The relative increases in antibody titer relative to the initial value are listed in Table 2. Qualitatively, the only significant immunogenic response depicted arose from the 2.0% functionalized SCK, **9**. The 0.5%, 1.0%, and 2.0% SCKs (**7**, **8**, and **9**) exhibited increases of 100% or more in 20% (1 of 5), 60% (3 of 5), and 100% (5 of 5) of the mice, respectively, following two booster injections.

While limited in scope, the immunogenicity results for the SCKs functionalized to a lesser degree are consistent

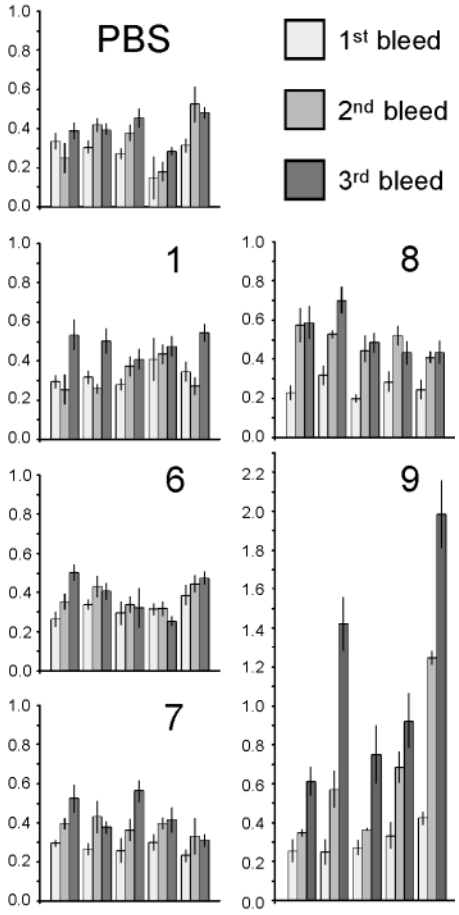

Figure 4. Each group of three bars within a data set corresponds to a titer measurement from an individual mouse. The red bars correspond to the prebleed, the orange bars represent the bleed two weeks after the 1st booster immunization, and the yellow bars represent the bleed two weeks following the 2nd booster immunization. Detrimental immunogenic effects, relative to controls, are negligible in all samples except for the 2.0% (**9**) sample, which suggests that the quantity of PTD and the manner in which it is presented on the surface have a synergistic effect that is able to produce an immune response significantly greater that the response elicited by the peptide itself. Error bars are representative of one standard deviation from the mean of triplicate samples harvested from two separate serum vials and are the estimates of the standard uncertainties.

Table 3. Relative Percent Increase in Antibody Titers Quantified by ELISA Following Two Booster Injections over Preimmunization Baseline Levels

	% increase after one booster over baseline levels mouse					% increase after two boosters over baseline levels mouse				
sample	**1**	**2**	**3**	**4**	**5**	**1**	**2**	**3**	**4**	**5**
1	6	34	-19	-14	-21	16	47	58	82	57
6	33	27	15	1	16	88	21	9	-19	23
7	34	63	41	32	43	78	43	118	39	33
8	153	66	124	84	68	158	121	147	53	80
9	36	130	34	106	194	140	475	177	178	368
PBS	-26	37	38	22	67	16	29	67	93	53

with the literature (*42*), but when large numbers of PTD are presented, the particles do elicit an increase in IgG concentration within the serum. While no specific responses could be detected for the any of the SCK nanoparticles, it is perhaps more important that no deaths resulted from the mice (>50) being subjected to the immunization protocol (three × 100 μg) and no gross morphological changes were observed in postmortem organ histology examinations.

CONCLUSIONS

SCK nanoparticles derivatized with various stoichiometric derivatizations with PTD have been evaluated in vitro and in vivo for biocompatibility. Although these data are somewhat limited in scope, the initial evaluation and early identification of detrimental interactions between biological species and SCK nanoparticles are crucial to further efforts to develop in vivo applications. Apoptosis assays measured by flow cytometry have complemented enzymatic (MTT) toxicity results demonstrating a lack of detrimental effects on cell viability below 500 mg/L for all the samples. Although higher levels of peptide functionalization resulted in decreased metabolic function, loss of cell viability was observed at a sufficiently high concentration, suggesting the use of even 2% PTD-functionalized SCKs would not be prohibited in vivo. In addition, RT-PCR data have provided quantitative information regarding the lack of immunogenicity elicited by SCKs and peptide-derivatized SCK nanoparticles. The inflammatory response to the peptide-functionalized SCK nanoparticles as measured by RT-PCR show increases in the levels of both TNF-α and IL1-β relative to TCPS. Although these levels are statistically significant and show large increases of IL1-β with increasing peptide functionalization, the levels did not preclude the preliminary testing of SCKs in vivo. An in vivo mouse immunization model found measured increases in IgG concentration were minimal with no specific interactions being identified, and more importantly, none of the mice (>50) subjected to the three 100 μg immunization protocol died. Additionally, no gross morphological changes were observed in postmortem organ histology examinations. While these in vitro assessments and preliminary in vivo tests show promising results, additional in vivo animal studies, which are currently in progress including biodistribution and nanoparticle clearance, are needed to compliment these initial findings and to extend the potential therapeutic applications of functionalized SCKs. However, up-regulation of IL1-β and larger than expected IgG increases for the 2.0% PTD-functionalized SCKs suggest that nanoparticles functionalized in polyvalent strategies may be interesting scaffolds for the attachment of known antigens for use in vaccination applications.

ACKNOWLEDGMENT

The authors gratefully acknowledge the National Cancer Institute (N01-CO-27103), and a Postdoctoral Fellowship (M.L.B.) from the National Research Council for supporting this research. Immunization, sera collections, and suggestions from Dan Piatchek and Jack Diani of the Washington University Department of Biology are gratefully acknowledged.

LITERATURE CITED

(1) Matyjaszewski, K., and Xia, J. (2001) Atom Transfer Radical Polymerization. *Chem. Rev. 101*, 2921−2990.

(2) Hawker, C. J., Bosman, A. W., and Harth, E. (2001) New Polymer Synthesis by Nitroxide Mediated Living Radical Polymerizations. *Chem. Rev. 101*, 3661−3688.

(3) Frechet, J. M. J. (2003) Dendrimers and Other Dendritic Macromolecules: From Building Blocks to Functional Assemblies in Nanoscience and Nanotechnology. *J. Polym. Sci., Part A: Polym. Chem. 41*, 3713−3725.

(4) Duncan, R. (2003) The Dawning Era of Polymer Therapeutics. *Nat. Rev. Drug Discovery 2*, 347−360.

(5) Nishiyama, N., Okazaki, S., Cabral, H., Miyamoto, M., Kato, Y., Sugiyama, Y., Nishio, K., Matsumura, Y., and Kataoka, K. (2003) Novel Cisplatin-incorporated Polymeric Micelles can Eradicate Solid Tumors in Mice. *Cancer Res. 63*, 8977−8983.

(6) Pan, D., Turner, J., and Wooley, K. L. (2003) Folic Acid-conjugated Nanostructured Materials Designed for Cancer Cell Targeting. *Chem. Commun*. 2400−2401.

(7) Haag, R. (2004) Supramolecular Drug-Delivery Systems Based on Polymeric Core−Shell Architectures. *Angew. Chem., Int. Ed. 43*, 278−282.

(8) Hubbell, J. A. (2003) Enhancing Drug Function. *Science 300*, 595−596.

(9) Moses, M. A., Brem, H., and Langer, R. (2003) Advancing the Field of Drug Delivery: Taking Aim at Cancer. *Cancer Cell 4*, 337−341.

(10) Kataoka, K., Harada, A., and Nagasaki, Y. (2001) Block Copolymer Micelles for Drug Delivery: Design, Characterization and Biological Significance. *Ad. Drug Delivery Rev. 47*, 113−131.

(11) Hubbell, J. A. (2003) Materials as Morphogenetic Guides in Tissue Engineering. *Curr. Opin. Biotechnol. 14*, 551−558.

(12) Bourke, S. L., and Kohn, J. (2003) Polymers Derived from the Amino Acid L-tyrosine: Polycarbonates, Polyarylates and Copolymers with Poly(ethylene glycol). *Adv. Drug Delivery Rev. 55*, 447−466.

(13) Wadia, J. S., and Dowdy, S. F. (2003) Modulation of Cellular Function by TAT Mediated Transduction of Full Length Proteins. *Curr. Protein Pept. Sci. 4*, 97−104.

(14) Beerens, A. M. J., Al Hadithy, A. F. Y., Rots, M. G., and Haisma, H. J. (2003) Protein Transduction Domains and the Utility in Gene Therapy. *Curr. Gene Ther. 3*, 486-494.

(15) Thurmond, K. B., II, Kowalewski, T., and Wooley, K. L. (1996) Water-Soluble Knedel-like Structures: The Preparation of Shell-Cross-Linked Small Particles. *J. Am. Chem. Soc. 118*, 7239−7240.

(16) Wooley, K. L. (2000) Shell Cross-linked Polymer Assemblies: Nanoscale Constructs Inspired from Biological Systems. *J. Polym. Sci., Part A: Polym. Chem. 38*, 1397−1407.

(17) Huang, H., Remsen, E. E., and Wooley, K. L. (1998) Amphiphilic Core−shell Nanospheres Obtained by Intramicellar Shell Cross-linking of Polymer Micelles with Poly(ethylene oxide) Linkers. *Chem. Commun. 13*, 1415−1416.

(18) Joralemon, M. J., Murthy, K. S., Remsen, E. E., Becker, M. L., and Wooley, K. L. (2004) Synthesis, Characterization, and Bioavailability of Mannosylated Shell Cross-linked Nanoparticles. *Biomacromolecules 5*, 903−913.

(19) Murthy, K. S., Ma, Q., Remsen, E. E., Kowalewski, T., and Wooley, K. L. (2003) Thermal Shaping of Shell-Cross-linked (SCK) Nanoparticles, Facilitated by Nanoconfinement of Fluidlike Cores. *J. Mater. Chem. 13*, 2785−2795.

(20) Remsen, E. E., Thurmond, K. B., II, and Wooley, K. L. (1999) Solution and Surface Charge Properties of Shell Cross-Linked Knedel Nanoparticles. *Macromolecules 32*, 3685−3689.

(21) Liu, J., Zhang, Q., Remsen, E. E., and Wooley, K. L. (2001) Bioconjugates of Protein Transduction Domain(PTD) and

Shell Cross-linked Nanoparticles: Nanostructured Materials Designed for Delivery into Cells. *Biomacromolecules 2*, 362−368.

(22) Green, M., and Loewenstein, P. (1988) Autonomous Functional Domains of Chemically Synthesized Human Immunodeficiency Virus TAT Trans-activator Protein. *Cell 55*, 1179−1188.

(23) Frankel, A., and Pabo, C. (1988) Cellular Uptake of the TAT Protein from Human Immunodeficiency Virus. *Cell 55*, 1189−1193.

(24) Wadia, J. S., and Dowdy, S. F. (2002) Protein Transduction Technology. *Curr. Opin. Biotechnol. 13*, 52.

(25) Nagahara, H., Vocero-Akbani, H. M., Snyder, E. L., Ho, A., Latham, D. G., Lissy, N. A., Becker-Hapak, M., Ezhevsky, S. A., and Dowdy, S. F. (1998) Transduction of Full-length TAT Fusion Proteins into Mammalian Cells: TAT-p27 Induces Cell Migration. *Nat. Med. 4*, 1449.

(26) Torchilin, V. P., Levchenko, T. S., Rammohan, R., Volodina, N., Papahadjopoulos-Sternberg, B., and D'Sousa, G. G. M. (2003) Cell Transfection in vitro and in vivo with Nontoxic TAT Peptide Liposome-DNA Complexes. *Proc. Natl. Acad. Sci. 100*, 1972−1977.

(27) Polyakov, V., Sharma, V., Dahlheimer, J. L., Pica, C. M., Luker, G. D., and Piwnica-Worms, D. (2000) Novel Tat-Peptide Chelates for Direct Transduction of Technetium-99m and Rhenium into Human Cells for Imaging and Radiotherapy. *Bioconjugate Chem. 11*, 762−771.

(28) Gammon, S. T., Villalobos, V. M., Prior, J. L., Sharma, V., and Piwnica-Worms, D. (2003) Quantitative Analysis of Permeatation Peptide Complexes Labeled with Technetium-99m: Chiral and Sequence-Specific Effects on Net Cell Uptake. *Bioconjugate Chem. 14*, 368−376.

(29) Bullok, K. E., Dyszlewski, M., Prior, J. L., Pica, C. M., Sharma, V., and Piwnica-Worms, D. (2002) Characterization of Novel Histidine-Tagged Tat-Peptide Complexes Dual-Labeled with 99mTc-Tricarbonyl and Fluorescein for Scintigraphy and Fluorescence Microscopy. *Bioconjugate Chem. 13*, 1226−1237.

(30) Hansen, M. B., E., N. S., and Berg, K. J. (1989). *J. Immunol. Methods 119*, 203−210.

(31) Catelas, I., Huk, O. L., Petit, A., Zukor, D. J., Marchand, R., and Yahida, L. H. (1998) Flow Cytometric Analysis of Macrophage Response to Ceramic and Polyethylene Particles: Effects of Size, Concentration, and Composition. *J. Biomed. Mater. Res. 41*, 600−607.

(32) Oppenheim, J. J. (2001) Cytokines: Past, Present, and Future. *Int. J. Hematol. 74*, 3−8.

(33) Wang, T., and Brown, M. J. (1999) mRNA Quantification by Real-time TaqMan Polymerase Chain Reaction: Validation and Comparison with RNase Protection. *Anal. Biochem. 269*, 198−201.

(34) Melton, D. A., Krieg, P. A., Rebagliati, M. R., Maniatis, T., Zinn, K., and Green, M. R. (1984) Efficient in vitro Synthesis of Biologically Active RNA and RNA Hybridization Probes from Plasmids Containing a Bacteriophage SP6 Promoter. *Nucleic Acids Res. 12*, 7035−7056.

(35) Morrison, T. B., Weis, J. J., and Wittwer, C. T. (1998) Quantification of Low-copy Transcripts by Continuous SYBR Green I Monitoring During Amplification. *Biotechniques 24*, 954−958.

(36) Bustin, S. A. (2000) Absolute Quantification of mRNA Using Real-time Reverse Transcription Polymerase Chain Reaction Assays. *J. Mol. Endocrinol. 25*, 169−193.

(37) Guatelli, J. C., Gingeras, T. R., and Richman, D. D. (1989) Nucleic Acid Amplification in vitro: Detection of Sequences with Low Copy Numbers and Application to Diagnosis of Human Immuno Deficiency Type 1 Infection. *Clin. Mirobiol. Rev. 2*, 217−226.

(38) Bailey, L., Washburn, N., Simon, C. G., Chan, E., and Wang, F. W. (2004) The Quantification of Inflammatory Cellular Responses Using Real-Time Polymerase Chain Reaction (RT-PCR). *J. Biomed. Mater. Res. 69*, 305−313.

(39) Bailey, L., Weir, M., and Washburn, N. (2004) The Quantification of Cellular Viability and Inflammatory Response to Dental Bonding Resins. *J. Dental Res.*, submitted.

(40) Brodbeck, W. G., Voskerician, G., Ziats, N. P., Nakayama, Y., Matsuda, T., and Anderson, J. M. (2003) In Vivo Leukocyte Cytokine mRNA Responses to Biomaterials are Dependent on Surface Chemistry. *J. Biomed. Mater. Res. 64*, 320−329.

(41) Suzuki, T., Futaki, S., Niwa, M., Tanaka, S., Ueda, K., and Sugiura, Y. (2002) Possible Existence of Common Internalization Mechanisms among Arginine Rich Peptides. *J. Biol. Chem. 277*, 2437−2443.

(42) Liefert, J. A., Harkins, S., and Whitton, J. L. (2002) Full-length Proteins Attached to the HIV tat Protein Transduction Domain are Neither Transduced between Cells, nor Exhibit Enhanced Immunogenicity. *Gene Ther. 9*, 1422−1428.

(43) Vassalli, P. (1992) The Pathophysiology of Tumor Necrosis Factors. *Annu. Rev. Immunol. 10*, 411−452.

(44) Kumar, V., Cotran, R. S., and Robbins, S. L. (1997) *Basic Pathology*, Saunders, New York.

(45) Beutler, B., and Cerami, A. (1988) Tumor Necrosis, Cachexia, Shock and Inflammation: A Common Mediator. *Annu. Rev. Biochem. 57*, 505−518.

(46) Cannon, J. G., and St. Pierre, B. A. (1998) Cytokines in Exertion Induced Skeletal Muscle Injury. *Mol. Cell Biochem. 179*, 159−167.

(47) Illei, G. G., and Lipsky, P. E. (2000) Novel, Antigen-specific Therapeutic Approaches to Autoimmune/ inflammatory Diseases. *Curr. Opin. Immunol. 12*, 712−718.

(48) Dai, Z., and Lakkis, F. G. (1999). *Curr. Opin. Immunol. 11*, 504−508.

(49) Giulietti, A., Overbergh, L., Valckx, D., Decallonne, B., Bouillon, R., and Mathieu, C. (2001) An Overview of Real-time Quantitative PCR: Applications to Quantify Cytokine Gene Expression. *Methods Enzymol. 25*, 386−401.

(50) Chapekar, M. S., Zaremba, T. G., Kuester, R. K., and Hitchins, V. M. (1996) Synergistic Induction of Tumor Necrosis Factor alpha by Bacterial Lipopolysaccharide and Lipoteichoic Acid in Combination with Polytetrafluoroethylene Particles in a Murine Macrophage Cell Line RAW 264.7. *J. Biomed. Mater. Res. 31*, 251−256.

(51) Funatogawa, K., Matsuura, M., Nakano, M., Kiso, M., and Hasegawa, A. (1998) Relationship of Structure and Biological Activity of Monosaccharide Lipid A Analogues to Induction of Nitric Oxide Production by Murine Macrophage RAW264.7 Cells. *Infect. Immun. 66*, 5792−5798.

(52) Jue, D. M., Sherry, B., Luedke, C., Manogue, K. R., and Cerami, A. (1990) Processing of Newly Synthesized Cachectin/ tumor Necrosis Factor in Endotoxin-stimulated Macrophages. *Biochemistry 29*, 8371−8377.

(53) Tiffany, C. W., and Burch, R. M. (1989) Bradykinin Stimulates Tumor Necrosis Factor and Interleukin-1 Release from Macrophages. *FEBS Lett 247*, 189−192.

(54) Suzuki, T., Higgins, P. J., and Crawford, D. R. (2000) Control Selection for RNA Quantitation. *Biotechniques 29*, 332−337.

(55) Filion, M. C., and Phillips, N. C. (1997) Toxicity and Immunomodulatory Activity of Liposomal Vectors Formulated with Cationic Lipids Toward Immune Effector Cells. *Biochim. Biophys. Acta 1329*, 345−356.

(56) Raabe, T., Bukrinsky, M., and Currie, R. A. (1998) Relative Contribution of Transcription and Translation to the Induction of Tumor Necrosis Factor-alpha by Lipopolysaccharide. *J. Biol. Chem. 273*, 974−980.

(57) Baer, M., Dillner, A., Schwartz, R. C., Sedon, C., Nedospasov, S., and Johnson, P. F. (1998) Tumor Necrosis Factor alpha Transcription in Macrophages is Attenuated by an Autocrine Factor that Preferentially Induces NF-kappaB p 50. *Mol. Cell Biol. 18*, 5678−5689.

(58) Tang, L., and Eaton, J. W. (1995) Inflammatory Responses to Biomaterials. *Am. J. Clin. Pathol. 103*, 466−471.

(59) "Official contribution of the National Institute of Standards and Technology; not subject to copyright in the United States."

BC049945M